

## Role of compressibility in moderating flame acceleration in tubes

Vitaly Bychkov,<sup>1</sup> Vyacheslav Akkerman,<sup>2,\*</sup> Damir Valiev,<sup>1</sup> and Chung K. Law<sup>2</sup>

<sup>1</sup>Department of Physics, Umeå University, S-901 87 Umeå, Sweden

<sup>2</sup>Department of Mechanical and Aerospace Engineering, Princeton University, Princeton, New Jersey 08544-5263, USA

(Received 10 September 2009; published 18 February 2010)

The effect of gas compression on spontaneous flame acceleration leading to deflagration-to-detonation transition is studied theoretically for small Reynolds number flame propagation from the closed end of a tube. The theory assumes weak compressibility through expansion in small Mach number. Results show that the flame front accelerates exponentially during the initial stage of propagation when the Mach number is negligible. With continuous increase in the flame velocity with respect to the tube wall, the flame-generated compression waves subsequently moderate the acceleration process by affecting the flame shape and velocity, as well as the flow driven by the flame.

DOI: 10.1103/PhysRevE.81.026309

PACS number(s): 47.70.Pq, 47.60.Dx, 47.40.-x, 47.63.mf

### I. INTRODUCTION

It has been widely observed [1–5] that a premixed flame propagating in a tube/channel from its closed end may spontaneously accelerate until detonation is triggered. However, the first quantitative theoretical result on this deflagration-to-detonation transition (DDT) phenomenon has only been obtained recently, with the assumption of gas incompressibility [6,7]. The theory yields the major parameters of the acceleration process such as the acceleration rate, the flame shape, and the velocity distribution ahead of the flame front. Furthermore, it also predicts the possibility of flame acceleration and DDT in microscale channels, which was recently observed experimentally in Ref. [8], thereby opens a new perspective in microscale combustion. At the same time, these experiments also demonstrated a number of possibilities in the acceleration process, which have not been found in the theory (see Fig. 1). *First*, the flame accelerates slower in the experiments than in an exponential growth regime identified in the theory. This also agrees with the numerical simulations [9,10], which demonstrated a nonexponential almost linear flame acceleration for moderate values of the Mach number. *Second*, at certain experimental conditions, the flame acceleration is followed by a “saturation” regime of fast steady deflagration, for which the deflagration wave propagates supersonically with respect to the tube walls but subsonically with respect to the fuel mixture just ahead of it. Experimental and numerical studies of flame acceleration and DDT in channels with obstacles [5,11–15] also indicated the importance of gas compression and the possibility of “fast” flames, which are supersonic in the laboratory reference frame and subsonic with respect to the fresh gas. They may be correlated with the Chapman-Jouguet (CJ) deflagration [16,17], whose high-subsonic speed implies the importance of compressibility in the propagation.

Subsequent numerical work [18] simulated the entire process of flame acceleration and DDT in smooth tubes from slow burning until explosion/detonation triggering. Figure 2

shows that the flame acceleration undergoes three distinctive stages: (1) initial exponential acceleration in a quasi-isobaric regime; (2) almost linear increase in the flame velocity, and as such almost constant acceleration, to near-sonic values; and (3) saturation to a quasisteady high-speed deflagration. It is emphasized that all these stages are related to *deflagration*, occurring *before* explosion and DDT, so this regime of fast quasisteady deflagration is not to be confused with detonation. Figure 2 also shows that this exponential regime of flame acceleration changes as soon as the flame velocity with respect to the tube walls becomes comparable to the sound speed, implying that the flame-generated compression waves would start to influence the flame propagation dynamics. Consequently, there is mounting evidence, both experimental and computational, that gas compression is important during the developed stages of flame acceleration.

The purpose of the present paper is therefore to analyze the role of gas compression in the acceleration process. We have extended the incompressible theory of flame acceleration, accounting for small but finite gas compression by employing expansion for small initial Mach numbers up to the first-order terms. We have determined how compression

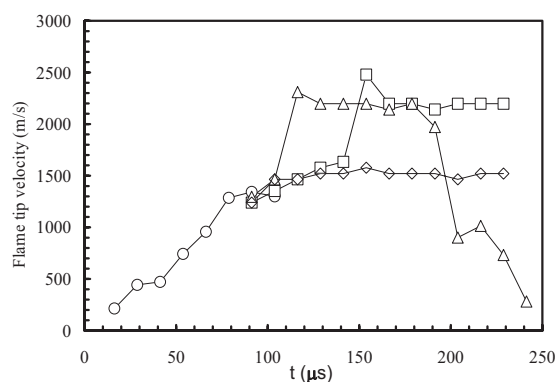


FIG. 1. Various possibilities of the acceleration process from the experiments in Ref. [8] on ethylene flames in a smooth capillary tube with 0.5 mm diameter: (□) DDT occurs and the reaction front travels at a near CJ detonation speed, (Δ) the detonation starts, but the detonation wave fails to propagate, and (◇) the flame accelerates to a constant speed.

\*Corresponding author. FAX: 1 609 258 6233; akkerman@princeton.edu

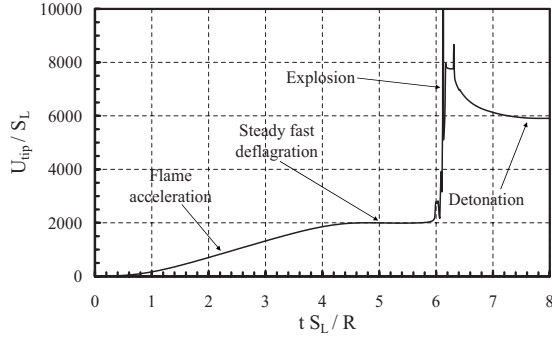


FIG. 2. Various stages of the flame acceleration and DDT from the simulations [18].

waves modify the regime of flame acceleration, the flame shape and velocity, as well as the flow driven by the flame, leading to the derivation of analytical expressions for the main characteristics of the flame dynamics. We have therefore demonstrated that flame-generated compression waves strongly moderate the flame acceleration and as such explained the recent experimental and numerical works on flame acceleration and DDT. The present theory is in good quantitative agreement with previous numerical simulations during the initial stage of flame acceleration when gas compression is relatively small. It also provides order-of-magnitude estimates in the regime of almost constant flame acceleration when gas compression is considerable and finally yields qualitative understanding of the process in the regime of fast quasisteady flame propagation.

The paper consists of five technical sections. In Secs. II and III we derive a set of equations governing evolution of the flame front and the flame-generated flow. The incompressible approach is summarized in Sec. II, while compressibility is accounted for in Sec. III. We solve the governing equations in Sec. IV and discuss the results in Sec. V.

## II. FLAME ACCELERATION IN AN INCOMPRESSIBLE FLOW

In this section we shall present the basic characteristics of flame acceleration in an incompressible flow. Figure 3 is a schematic of the problem under study. Here a laminar flame propagates from the closed end of a semi-infinite two-dimensional channel of half-width  $R$  with adiabatic nonslip walls. The  $z$  axis is directed along the wall and the  $x$  axis is perpendicular to it. Mechanistically, thermal expansion of the burned gas produces a flow ahead of the flame, which becomes nonuniform because of wall friction. This, in turn,

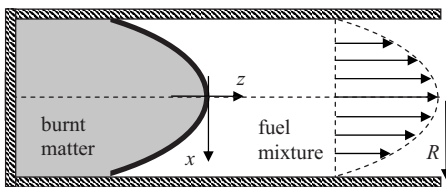


FIG. 3. Typical configuration of a flame propagating from the closed end of a tube or channel.

renders the flame front curved and leads to its acceleration.

We adopt the conventional approach of an infinitely thin flame propagating locally with the normal velocity  $S_L$  with respect to the unburned gas. Then, the total burning rate  $U_w$  is proportional to the entire flame surface area. In addition, we assume a quiescent burnt gas and a plane-parallel flow of the fuel mixture. It is noted that the plane-parallel flow is an approximation [6,7] because curvature of the flame front would induce transverse fluxes.

We shall use the scaled variables  $\eta=x/R$ ,  $\xi=z/R$ ,  $\mathbf{w}=\mathbf{u}/S_L$ ,  $\Omega_w=U_w/S_L$ , and  $\tau=tS_L/R$ , with the density and pressure scaled by  $\rho_0$  and  $\rho_0 S_L^2$ , respectively. Viscosity is characterized by the Reynolds number related to flame propagation,  $\text{Re}=S_L R/\nu$ , where  $\nu$  is the kinematical viscosity. The assumption of a plane-parallel flow  $\mathbf{w}=\hat{e}_z w(\eta, \tau)$  is self-consistent if the pressure gradient is a function of time only. Then the Navier-Stokes equation ahead of the flame reads

$$\frac{\partial w_a}{\partial \tau} = \Pi(\tau) + \frac{1}{\text{Re}} \frac{\partial^2 w_a}{\partial \eta^2}, \quad (1)$$

where the term  $\Pi=-\rho^{-1} \partial P/\partial \xi$  is produced by flame propagation, which acts on the fuel mixture as a semitransparent piston moving with the scaled velocity  $\Omega_w$  with respect to the fuel mixture and the subscript  $a$  designates the flow ahead of the flame front. Due to thermal expansion across the flame, the dimensionless gas volume increases by an amount  $(\Theta-1)\Omega_w$  per unit time, where

$$\Theta \equiv \frac{\rho_0}{\rho_b} = \frac{T_b}{T_0} = 1 + \frac{Q}{C_p T_0} \quad (2)$$

is the expansion factor,  $Q$  is the energy release from the reaction, and  $C_p$  is the heat capacity at constant pressure. Then the instantaneous average velocity of the fuel mixture is

$$\langle w \rangle_a = (\Theta - 1)\Omega_w, \quad (3)$$

where  $\langle \dots \rangle$  designates averaging over the entire channel width. The scaled flame position is described by

$$\xi_f(\eta, \tau) = \xi_{tip}(\tau) - f(\eta, \tau), \quad (4)$$

where  $\xi_{tip} \equiv \xi_f(0, \tau)$  denotes the flame tip, at the channel axis, and  $f(\eta, \tau)$  describes the flame shape, with  $f(0, \tau)=0$  by definition. The local burning rate is proportional to the local increase in the flame surface area,  $\sqrt{1+(\partial f/\partial \eta)^2}$ . In addition, the flame is drifted by the flow. Consequently, the flame evolution equation is described by

$$\frac{\partial \xi_f}{\partial \tau} = w_a + \sqrt{1 + \left(\frac{\partial f}{\partial \eta}\right)^2}. \quad (5)$$

Due to the flame acceleration, after a short time we have  $(\partial f/\partial \eta)^2 \gg 1$  everywhere except for the flat region close to the channel axis. We can therefore approximate Eq. (5) by the linear relation

$$\frac{\partial \xi_f}{\partial \tau} = w_a + \frac{\partial f}{\partial \eta}, \quad (6)$$

which yields a linear equation for the flame shape

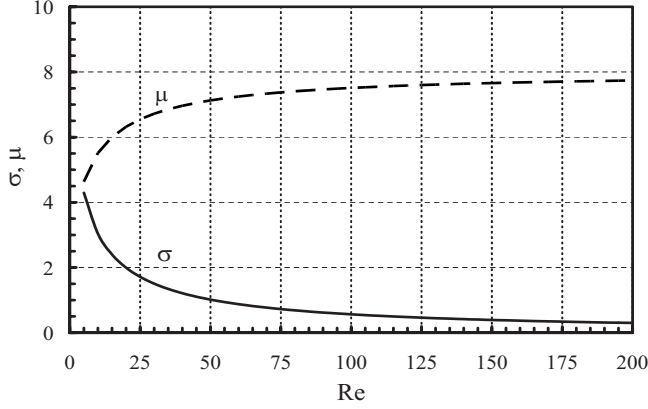


FIG. 4. The acceleration exponent  $\sigma$  [Eq. (10)] and the parameter  $\mu = \sqrt{\sigma} \text{Re}$  versus the Reynolds number related to flame propagation,  $\text{Re} = S_L R / \nu$ , with thermal expansion  $\Theta = 8$ .

$$\frac{\partial f}{\partial \tau} + \frac{\partial f}{\partial \eta} = w_a(0, \tau) - w_a(\eta, \tau), \quad (7)$$

with  $\partial f / \partial \eta \geq 0$  for a convex flame. We also define the average flame position  $\bar{\Sigma} = \langle \xi_f \rangle$ , which is related to the flame velocity in the laboratory reference frame  $U_L$  as  $\dot{\bar{\Sigma}} = U_L / S_L$ . Averaging Eq. (6) yields

$$\dot{\bar{\Sigma}} = \langle w \rangle_a + \Omega_w = \langle w \rangle_a + \int_0^1 \frac{\partial f}{\partial \eta} d\eta = \langle w \rangle_a + f(1, \tau). \quad (8)$$

According to Eqs. (3) and (8), we have  $\dot{\bar{\Sigma}} = \Theta \Omega_w$  or  $U_L = \Theta U_w$  for an incompressible flow.

The set of Eqs. (1), (3), (7), and (8) was solved analytically and substantiated by extensive numerical simulations [6]. It was shown that, asymptotically in time, the flame accelerates exponentially as

$$\Omega_w \propto \exp(\sigma S_L t / R), \quad (9)$$

with the acceleration rate

$$\sigma = \frac{(\text{Re} - 1)^2}{4\text{Re}} \left[ \sqrt{1 + \frac{4\text{Re}\Theta}{(\text{Re} - 1)^2}} - 1 \right]^2. \quad (10)$$

The theoretical prediction [Eq. (10)] for  $\Theta = 8$  is shown in Fig. 4 by the solid line. We observe that the acceleration rate decreases strongly with the channel width or more generally the Reynolds number. Such a dependence can be clearly demonstrated by noting that in the limit of large  $\text{Re}$ ,  $\text{Re} \gg 4\Theta$ , Eq. (10) yields  $\sigma = \Theta^2 / \text{Re}$ , which also shows that the acceleration rate increases with thermal expansion. Analytical expressions for the self-similar flame shape and the velocity profile were also found and were presented in Sec. IV as the zeroth-order solution.

### III. EFFECTS OF COMPRESSIBILITY ON THE FLAME-GENERATED FLOW

Now we study the effects of compressibility through first-order approximation in the initial Mach number related to flame propagation,  $M_0 \equiv S_L / c_0 \ll 1$ , where  $c_0 = c(T_0)$  is the

initial sound speed of the fuel mixture. In order to describe a compression wave, we shall neglect the multidimensional flame structure by approximating the flame front as a one-dimensional (1D) surface of the locus  $\Sigma = \Sigma(t)$ . In the limit of weak compression, isentropic approximation may be adopted. Then, the scaled density  $\zeta = \rho / \rho_0$ , pressure  $p = P / P_0$ , and temperature  $\vartheta = T / T_0$  just ahead of the flame are given by [16]

$$\begin{aligned} \zeta_a &= \left( 1 + \frac{\gamma - 1}{2} M_0 \langle w \rangle_a \right)^{2/(\gamma - 1)} \\ &= 1 + M_0 \langle w \rangle_a + \frac{3 - \gamma}{4} M_0^2 \langle w \rangle_a^2 + \dots \\ &\approx 1 + M_0 \langle w \rangle_a, \end{aligned} \quad (11)$$

$$\begin{aligned} p_a &= \left( 1 + \frac{\gamma - 1}{2} M_0 \langle w \rangle_a \right)^{2\gamma/(\gamma - 1)} \\ &= 1 + \gamma M_0 \langle w \rangle_a + \frac{\gamma(\gamma + 1)}{4} M_0^2 \langle w \rangle_a^2 + \dots \\ &\approx 1 + \gamma M_0 \langle w \rangle_a, \end{aligned} \quad (12)$$

$$\begin{aligned} \vartheta_a &= \left( 1 + \frac{\gamma - 1}{2} M_0 \langle w \rangle_a \right)^2 \\ &= 1 + (\gamma - 1) M_0 \langle w \rangle_a + \frac{(\gamma - 1)^2}{4} M_0^2 \langle w \rangle_a^2 + \dots \\ &\approx 1 + (\gamma - 1) M_0 \langle w \rangle_a, \end{aligned} \quad (13)$$

where  $\gamma = C_p / C_v$  is the adiabatic exponent. Equations (11)–(13) also determine the rigorous mathematical limit of validity for the present theory:  $M_0^2 \langle w \rangle_a^2 \ll 4 / \gamma(\gamma + 1)$ . Indeed, this limit is violated when the second-order terms in Eqs. (11)–(13), neglected in the theory, become important. Matching conditions at the flame front take the form

$$\zeta_a(\dot{\bar{\Sigma}} - \langle w \rangle_a) = \zeta_{bf}(\dot{\bar{\Sigma}} - \langle w \rangle_{bf}), \quad (14)$$

$$p_a + \gamma M_0^2 \zeta_a (\dot{\bar{\Sigma}} - \langle w \rangle_a)^2 = p_{bf} + \gamma M_0^2 \zeta_{bf} (\dot{\bar{\Sigma}} - \langle w \rangle_{bf})^2, \quad (15)$$

$$\begin{aligned} \vartheta_a + \Theta - 1 + \frac{\gamma - 1}{2} M_0^2 (\dot{\bar{\Sigma}} - \langle w \rangle_a)^2 \\ = \vartheta_{bf} + \frac{\gamma - 1}{2} M_0^2 (\dot{\bar{\Sigma}} - \langle w \rangle_{bf})^2, \end{aligned} \quad (16)$$

where the subscript  $bf$  denotes the burnt gas just behind the flame front and  $\Theta$  stands for the initial expansion factor, given by Eq. (2). To first-order approximation in  $M_0$ , Eqs. (15) and (16) and the perfect gas law yield

$$p_{bf} = p_a, \quad \vartheta_{bf} = \vartheta_a + \Theta - 1, \quad \zeta_{bf} = \zeta_a / \theta, \quad (17)$$

where

$$\theta \equiv \frac{\vartheta_{bf}}{\vartheta_a} = 1 + \frac{\Theta - 1}{\vartheta_a} \quad (18)$$

is the expansion factor accounting for compressibility. Obviously,  $\theta = \Theta$  when compression is negligible and  $M_0 \langle w \rangle_a \rightarrow 0$ . However,  $\vartheta_a$  increases and  $\theta$  reduces as soon as the flame accelerates, hence moderating the flame acceleration.

For the flow in the burnt gas, from the continuity equation

$$\frac{\partial \zeta_b}{\partial \tau} + \frac{\partial}{\partial \xi} (\zeta_b w_b) = 0, \quad (19)$$

and the condition of adiabatic compression,  $p \propto \zeta^\gamma$ , we find

$$\frac{\partial w_b}{\partial \xi} = - \frac{1}{\zeta_b} \frac{d\zeta_b}{d\tau} = - \frac{1}{\gamma p_b} \frac{dp_b}{d\tau}, \quad (20)$$

where the substantial derivative is taken for a particular gas parcel.

For the same 1D model, we have another equation for pressure [16],

$$M_0^2 \left( \frac{\partial w_b}{\partial \tau} + w_b \frac{\partial w_b}{\partial \xi} \right) = - \frac{1}{\zeta_b} \frac{\partial p_b}{\partial \xi}. \quad (21)$$

Neglecting the second-order term of  $M_0$  in Eq. (21), we obtain a uniform pressure distribution in the burnt gas. Consequently, pressure is a function of time only,  $p_b = p_{bf}(\tau) = p_a(\tau)$ . Then Eq. (20) can be readily integrated as

$$w_b = - \frac{1}{\gamma p_a} \frac{dp_a}{d\tau} \xi, \quad (22)$$

with

$$w_{bf} = - \frac{1}{\gamma p_a} \frac{dp_a}{d\tau} \Sigma \quad (23)$$

just behind the flame front. Finally, substituting Eqs. (12), (13), (17), (18), and (23) into Eq. (14), we have to the first-order approximation in  $M_0$

$$\langle w \rangle_a = \frac{\Theta - 1}{\Theta} \left[ \dot{\Sigma} - (\gamma - 1) M_0 \frac{\Theta - 1}{\Theta^2} (\dot{\Sigma})^2 - \frac{M_0}{\Theta} \ddot{\Sigma} \right]. \quad (24)$$

Equation (24) describes the instantaneous average velocity of the flow generated by an accelerating flame. In the limit of an incompressible flow,  $M_0 \rightarrow 0$ , Eq. (24) reduces to Eq. (3). Equations (1), (7), (8), and (24) then describe the flame acceleration and the flame-generated flow in a semi-infinite channel with nonslip adiabatic walls.

#### IV. FLAME ACCELERATION IN A COMPRESSIBLE FLOW

In this section we shall solve the set of Eqs. (1), (7), (8), and (24). First, we look for a velocity profile in the form

$$w_a(\eta, \tau) = \alpha_1(\eta) \exp(\sigma\tau) + M_0 \alpha_2(\eta) \exp(2\sigma\tau). \quad (25)$$

Substituting Eq. (25) into Eq. (1), we split the problem as

$$\frac{d^2 \alpha_1}{d\eta^2} = \mu^2 \alpha_1 - \pi_1(\tau), \quad (26)$$

$$\frac{d^2 \alpha_2}{d\eta^2} = 2\mu^2 \alpha_2 - \pi_2(\tau), \quad (27)$$

where  $\mu \equiv \sqrt{\sigma \text{Re}}$ ,  $\alpha_1(\eta)$  and  $\alpha_2(\eta)$  are even functions with the boundary conditions at the walls  $\alpha_1(\pm 1) = \alpha_2(\pm 1) = 0$ , and  $\pi_1(\tau)$  and  $\pi_2(\tau)$  are such functions that

$$\Pi(\tau) = \frac{1}{\text{Re}} [\pi_1(\tau) \exp(\sigma\tau) + M_0 \pi_2(\tau) \exp(2\sigma\tau)]. \quad (28)$$

The solution to Eqs. (26) and (27) takes the form

$$\alpha_1(\eta) = \langle \alpha_1 \rangle \frac{\cosh \mu - \cosh(\mu\eta)}{\cosh \mu - \mu^{-1} \sinh \mu}, \quad (29)$$

$$\alpha_2(\eta) = \langle \alpha_2 \rangle \frac{\cosh(\sqrt{2}\mu) - \cosh(\sqrt{2}\mu\eta)}{\cosh(\sqrt{2}\mu) - (\sqrt{2}\mu)^{-1} \sinh(\sqrt{2}\mu)}. \quad (30)$$

Similar to Eq. (25), we look for a flame shape in the form

$$f(\eta, \tau) = \Phi_1(\eta) \exp(\sigma\tau) + M_0 \Phi_2(\eta) \exp(2\sigma\tau). \quad (31)$$

Substituting Eq. (31) into Eq. (7), we split the latter into two equations,

$$\sigma \Phi_1 + \frac{d\Phi_1}{d\eta} = \alpha_1(0) - \alpha_1(\eta) = \langle \alpha_1 \rangle \frac{\cosh(\mu\eta) - 1}{\cosh \mu - \mu^{-1} \sinh \mu}, \quad (32)$$

$$\begin{aligned} 2\sigma \Phi_2 + \frac{d\Phi_2}{d\eta} &= \alpha_2(0) - \alpha_2(\eta) \\ &= \langle \alpha_2 \rangle \frac{\cosh(\sqrt{2}\mu\eta) - 1}{\cosh(\sqrt{2}\mu) - (\sqrt{2}\mu)^{-1} \sinh(\sqrt{2}\mu)}, \end{aligned} \quad (33)$$

with the solutions

$$\begin{aligned} \Phi_1(\eta) &= \frac{\langle \alpha_1 \rangle \exp(-\sigma\eta)}{\cosh \mu - \mu^{-1} \sinh \mu} \int_0^\eta [\cosh(\mu\chi) - 1] \exp(\sigma\chi) d\chi \\ &= \frac{\langle \alpha_1 \rangle}{\cosh \mu - \mu^{-1} \sinh \mu} \left\{ \frac{\exp(\mu\eta)}{2(\mu + \sigma)} - \frac{\exp(-\mu\eta)}{2(\mu - \sigma)} \right. \\ &\quad \left. + \frac{1}{\sigma} \left[ \frac{\mu^2}{\mu^2 - \sigma^2} \exp(-\sigma\eta) - 1 \right] \right\}, \end{aligned} \quad (34)$$

$$\begin{aligned} \Phi_2(\eta) &= \frac{\langle \alpha_2 \rangle \exp(-2\sigma\eta)}{\cosh(\sqrt{2}\mu) - (\sqrt{2}\mu)^{-1} \sinh(\sqrt{2}\mu)} \\ &\quad \times \int_0^\eta [\cosh(\sqrt{2}\mu\chi) - 1] \exp(2\sigma\chi) d\chi \\ &= \frac{1}{2} \frac{\langle \alpha_2 \rangle}{\cosh(\sqrt{2}\mu) - (\sqrt{2}\mu)^{-1} \sinh(\sqrt{2}\mu)} \\ &\quad \times \left\{ \frac{\exp(\sqrt{2}\mu\eta)}{\sqrt{2}\mu + 2\sigma} - \frac{\exp(-\sqrt{2}\mu\eta)}{\sqrt{2}\mu - 2\sigma} \right\} \end{aligned}$$

$$+ \frac{1}{\sigma} \left[ \frac{\mu^2}{\mu^2 - 2\sigma^2} \exp(-2\sigma\eta) - 1 \right] \Bigg\}. \quad (35)$$

It is convenient to introduce the coefficients

$$S_1 = \left\{ \frac{\exp(\mu)}{2(\mu + \sigma)} - \frac{\exp(-\mu)}{2(\mu - \sigma)} + \frac{1}{\sigma} \left[ \frac{\mu^2}{\mu^2 - \sigma^2} \exp(-\sigma) - 1 \right] \right\} \\ \times [\cosh \mu - \mu^{-1} \sinh \mu]^{-1}, \quad (36)$$

$$S_2 = \frac{1}{2} \left\{ \frac{\exp(\sqrt{2}\mu)}{\sqrt{2}\mu + 2\sigma} - \frac{\exp(-\sqrt{2}\mu)}{\sqrt{2}\mu - 2\sigma} + \frac{1}{\sigma} \left[ \frac{\mu^2}{\mu^2 - 2\sigma^2} \right. \right. \\ \left. \left. \times \exp(-2\sigma) - 1 \right] \right\} \\ \times [\cosh(\sqrt{2}\mu) - (\sqrt{2}\mu)^{-1} \sinh(\sqrt{2}\mu)]^{-1}. \quad (37)$$

Then  $\Phi_1(1) = \langle \alpha_1 \rangle S_1$ ,  $\Phi_2(1) = \langle \alpha_2 \rangle S_2$ , and, according to Eqs. (8), (25), and (31), we have

$$\dot{\Sigma} = \langle \alpha_1 \rangle (1 + S_1) \exp(\sigma\tau) + M_0 \langle \alpha_2 \rangle (1 + S_2) \exp(2\sigma\tau), \quad (38)$$

with

$$\Sigma = \frac{\langle \alpha_1 \rangle}{\sigma} (1 + S_1) \exp(\sigma\tau) + M_0 \frac{\langle \alpha_2 \rangle}{2\sigma} (1 + S_2) \exp(2\sigma\tau), \quad (39)$$

$$\ddot{\Sigma} = \sigma \langle \alpha_1 \rangle (1 + S_1) \exp(\sigma\tau) + 2M_0 \sigma \langle \alpha_2 \rangle (1 + S_2) \exp(2\sigma\tau). \quad (40)$$

Finally, substituting Eqs. (25) and (38)–(40) into Eq. (24) and equating the zeroth- and first-order modes, respectively, we find

$$\frac{\Theta - 1}{\Theta} (1 + S_1) = 1, \quad (41)$$

$$\langle \alpha_2 \rangle = -A \langle \alpha_1 \rangle^2, \quad (42)$$

where

$$A = \left[ \frac{\gamma - 1}{\Theta} + \frac{1}{\Theta - 1} \right] \frac{\Theta}{1 - (\Theta - 1)S_2}. \quad (43)$$

The zeroth-order equations [Eqs. (3), (29), (34), and (41)] reproduce the theory of flame acceleration in an incompressible flow [6], with Eq. (3) describing the amplitude  $\langle \alpha_1 \rangle$  through  $\langle \alpha_1 \rangle = \Theta - 1$ , Eq. (29) describing the incompressible flow velocity profile, Eq. (34) describing the flame shape, and Eq. (41) describing the parameter  $\sigma$ . In the limit of  $\mu \gg 1$ , Eq. (36) reduces to

$$S_1 \approx \frac{\mu}{(\mu - 1)(\mu + \sigma)} = \frac{1}{\Theta - 1}, \quad (44)$$

which leads to Eq. (10). The dashed plot in Fig. 4 shows the parameter  $\mu$  versus Re for  $\Theta = 8$ . We observe that  $\mu$  increases slowly and tends to the saturation value  $\mu = \Theta$  at  $\text{Re} \gg 4\Theta$ .

The limit of  $\exp(-\mu) \ll 1$ ,  $\exp(-\sigma) \ll 1$  holds with good accuracy for flames with thermal expansion  $\Theta = 5 - 8$ . Consequently, Eq. (44) reproduces Eq. (36) quite well.

Equations (30) and (35) then yield first-order corrections to the flow velocity profile and the flame shape, respectively, while Eqs. (42) and (43) determine the relation between  $\langle \alpha_1 \rangle$  and  $\langle \alpha_2 \rangle$ . Keeping the same accuracy as that of Eq. (44), we approximate Eq. (37) as

$$S_2 \approx \frac{\mu}{(\sqrt{2}\mu - 1)(\mu + \sqrt{2}\sigma)}. \quad (45)$$

Then, one can readily check from Eqs. (44) and (45) that  $S_2 < S_1$  and  $S_2(\Theta - 1) < 1$  for any  $\mu$ . Consequently,  $A > 0$ , and the value  $\langle \alpha_2 \rangle = -A(\Theta - 1)^2$  is negative, which means that the first-order corrections lead to moderation of the flame acceleration.

We next express the velocity profile and flame shape as

$$w_a(\eta, \tau) = (\Theta - 1) \frac{\cosh \mu - \cosh(\mu\eta)}{\cosh \mu - \mu^{-1} \sinh \mu} \exp(\sigma\tau) \\ - M_0 (\Theta - 1)^2 A \frac{\cosh(\sqrt{2}\mu) - \cosh(\sqrt{2}\mu\eta)}{\cosh(\sqrt{2}\mu) - (\sqrt{2}\mu)^{-1} \sinh(\sqrt{2}\mu)} \\ \times \exp(2\sigma\tau), \quad (46)$$

$$f(\eta, \tau) = \frac{(\Theta - 1) \exp(\sigma\tau)}{\cosh \mu - \mu^{-1} \sinh \mu} \left\{ \frac{\exp(\mu\eta)}{2(\mu + \sigma)} - \frac{\exp(-\mu\eta)}{2(\mu - \sigma)} \right. \\ \left. + \frac{1}{\sigma} \left[ \frac{\mu^2}{\mu^2 - \sigma^2} \exp(-\sigma\eta) - 1 \right] \right\} \\ - \frac{1}{2} \frac{M_0 (\Theta - 1)^2 A \exp(2\sigma\tau)}{\cosh(\sqrt{2}\mu) - (\sqrt{2}\mu)^{-1} \sinh(\sqrt{2}\mu)} \\ \times \left\{ \frac{\exp(\sqrt{2}\mu\eta)}{\sqrt{2}\mu + 2\sigma} - \frac{\exp(-\sqrt{2}\mu\eta)}{\sqrt{2}\mu - 2\sigma} + \frac{1}{\sigma} \left[ \frac{\mu^2}{\mu^2 - 2\sigma^2} \right. \right. \\ \left. \left. \times \exp(-2\sigma\eta) - 1 \right] \right\}. \quad (47)$$

Furthermore, for large expansion we have  $\mu \gg 1$ ,  $\mu\eta \gg 1$  almost everywhere in the channel, so Eqs. (46) and (47) can be simplified as

$$w_a(\eta, \tau) = (\mu + \sigma) \{1 - \exp[\mu(\eta - 1)]\} \\ \times \exp(\sigma\tau) - M_0 (\Theta - 1)^2 A S_2 (\sqrt{2}\mu + 2\sigma) \\ \times \{1 - \exp[\sqrt{2}\mu(\eta - 1)]\} \exp(2\sigma\tau), \quad (48)$$

$$f(\eta, \tau) = \exp[\mu(\eta - 1)] \exp(\sigma\tau) - M_0 (\Theta - 1)^2 A S_2 \\ \times \exp[\sqrt{2}\mu(\eta - 1)] \exp(2\sigma\tau). \quad (49)$$

Equations (48) and (49) fail around the channel axis, where  $\eta \cong 0$ . This limitation, however, induces only an exponentially small error to the flame velocity and position. Averaging Eq. (46), we find

$$\langle w \rangle_a = (\Theta - 1) \exp(\sigma\tau) - M_0 A (\Theta - 1)^2 \exp(2\sigma\tau). \quad (50)$$

Then, to the first-order approximation in  $M_0$ , the scaled density, pressure, and temperature just ahead of the flame front take the form

$$\zeta_a = 1 + M_0 (\Theta - 1) \exp(\sigma\tau), \quad (51)$$

$$p_a = 1 + \gamma M_0 (\Theta - 1) \exp(\sigma\tau), \quad (52)$$

$$\vartheta_a = 1 + (\gamma - 1) M_0 (\Theta - 1) \exp(\sigma\tau). \quad (53)$$

We recall that the limit of validity for the present theory is  $M_0^2 \langle w \rangle_a^2 \ll 4 / \gamma(\gamma + 1)$ . According to Eq. (50), this limit corresponds to  $\sigma\tau \approx 4$  for  $\gamma = 1.4$  and  $M_0 = 10^{-3}$ .

The average flame position and the total burning rate are given by

$$\Sigma = \frac{\Theta}{\sigma} \exp(\sigma\tau) - M_0 \frac{(\Theta - 1)^2}{2\sigma} A (1 + S_2) \exp(2\sigma\tau), \quad (54)$$

$$\dot{\Sigma} = \Theta \exp(\sigma\tau) - M_0 (\Theta - 1)^2 A (1 + S_2) \exp(2\sigma\tau), \quad (55)$$

respectively. As for the position and velocity of the flame tip, Eqs. (4), (49), and (55) yield

$$\xi_{tip} = \Sigma + \langle f \rangle = \left( \frac{\Theta}{\sigma} + \frac{1}{\mu} \right) \exp(\sigma\tau) - M_0 \frac{(\Theta - 1)^2 A}{2\sigma} \times \left[ 1 + S_2 \left( 1 + \sqrt{2} \frac{\sigma}{\mu} \right) \right] \exp(2\sigma\tau), \quad (56)$$

$$\dot{\xi}_{tip} = \dot{\Sigma} + \langle \dot{f} \rangle = \left( \Theta + \frac{\sigma}{\mu} \right) \exp(\sigma\tau) - M_0 (\Theta - 1)^2 A \times \left[ 1 + S_2 \left( 1 + \sqrt{2} \frac{\sigma}{\mu} \right) \right] \exp(2\sigma\tau). \quad (57)$$

## V. DISCUSSION

In Sec. IV evolution of the velocity profile [Eq. (48)], average flow velocity [Eq. (50)], density [Eq. (51)], pressure [Eq. (52)], and temperature [Eq. (53)], as well as the flame shape [Eq. (49)], position [Eqs. (54) and (56)], and velocity [Eqs. (55) and (57)], have been determined. We observe that the flame tip velocity and position reproduce well the average flame speed and position. Indeed, for large Reynolds numbers Eqs. (10) and (54)–(57) yield

$$\dot{\xi}_{tip} \approx \left( 1 + \frac{1}{\text{Re}} \right) \dot{\Sigma} \approx \dot{\Sigma}, \quad \xi_{tip} \approx \left( 1 + \frac{1}{\text{Re}} \right) \Sigma \approx \Sigma. \quad (58)$$

Equations (48)–(57) provide first-order corrections to incompressible solutions, which show exponential acceleration. As we can see, the absolute values of the first-order terms, though small during the first stage, grow as fast as  $\exp(2\sigma\tau)$  and become progressively more important with time. Since all these terms are negative, they induce moderation in the flame acceleration due to gas compressibility. We emphasize that since  $\sigma$  remains the governing parameter of flame propa-

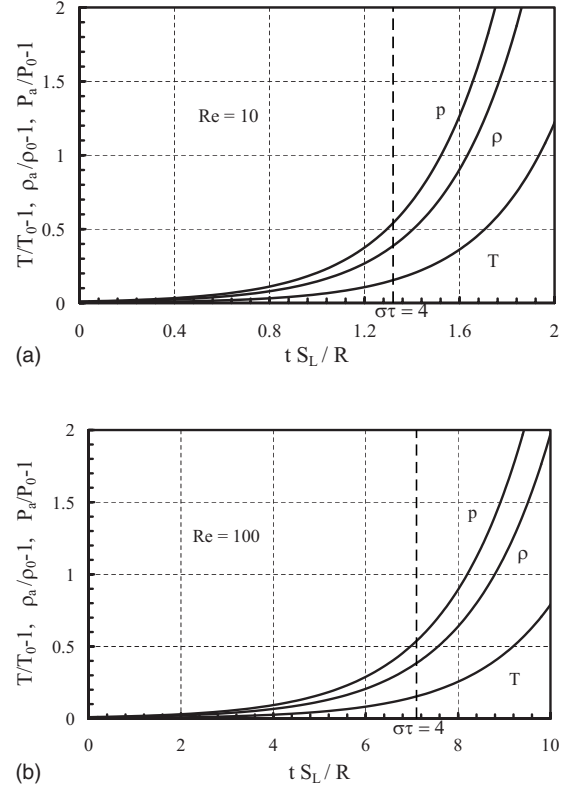


FIG. 5. Time evolution of the scaled density  $\rho_a/\rho_0$  [Eq. (51)], pressure  $P_a/P_0$  [Eq. (52)], and temperature  $T/T_0$  [Eq. (53)] just ahead of the flame front for  $\Theta=8$ ,  $\gamma=1.4$  and (a)  $\text{Re}=10$  and (b)  $\text{Re}=100$ . The vertical line is related to the validity limit  $\sigma\tau \approx 4$ .

gation even in a compressible flow, the flame acceleration becomes stronger with thermal expansion and weaker with the channel width both in the zeroth- and first-order approximations in  $M_0$ .

Time evolution of the scaled density, pressure, and temperature just ahead of the flame front [Eqs. (51)–(53)] are shown in Fig. 5(a) for  $\text{Re}=10$  and in Fig. 5(b) for  $\text{Re}=100$ , with the initial expansion factor  $\Theta=8$  and the adiabatic exponent  $\gamma=1.4$ . The vertical line is related to the validity limit  $\sigma\tau \approx 4$ .

It is noted that the increase in the upstream temperature and pressure as a result of compression also influences the unstretched laminar flame speed as  $S_L \propto p_a^{n/2-1} \vartheta_a \exp[\kappa(\vartheta_a - 1)]$ , where  $n$  is the global reaction order and the exponential factor  $\kappa$  is of the order of unity [3,19]. It has been demonstrated both experimentally and computationally [19] that the pressure dependence of the reaction rate for realistic fuels is greatly affected by the essential presence of the three-body termination elementary reactions such that  $n$  is frequently close to or even less than unity instead of the idealized value of two for a fuel-oxidizer system dominated by second-order branching and carrying elementary reactions. As such, for a 15% increase in the upstream temperature and 50% increase in pressure due to compression at the validity limit, the change in the laminar flame speed is negligible, being at most a few percent. Consequently, in the present work the flame speed is assumed to be a constant at its original value.

The velocity profile in the fuel mixture [Eq. (48)] is shown in Fig. 6(a) for  $\text{Re}=10$  at the instants  $t S_L/R$

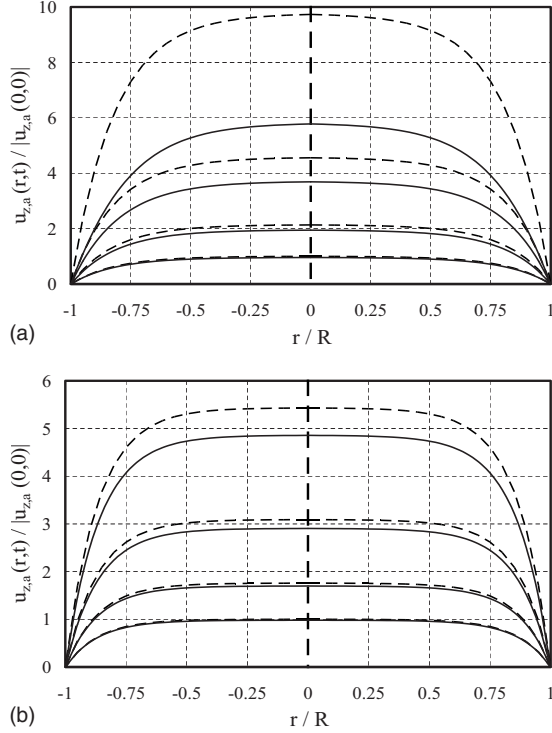


FIG. 6. Scaled velocity profile ahead of the flame [Eq. (48)] (a) for  $Re=10$  at the instants  $tS_L/R=0, 0.25, 0.5, 0.75$  and (b) for  $Re=100$  at the instants  $tS_L/R=0, 1, 2, 3$ , with the initial expansion factor  $\Theta=8$  and the adiabatic exponent  $\gamma=1.4$ .

$=0, 0.25, 0.5, 0.75$  and in Fig. 6(b) for  $Re=100$  at the instants  $tS_L/R=0, 1, 2, 3$ , with the expansion factor  $\Theta=8$  and the adiabatic exponent  $\gamma=1.4$ . The dashed plots are for the incompressible flow,  $M_0=0$ , while the solid plots present the compressible results given by Eq. (48) with  $M_0=10^{-3}$ . We observe that the velocity amplitude increases much faster in the incompressible approximation than that for the compressible flow and that the effects of gas compression are more pronounced in channels with less  $Re$ . Figure 7 is a counterpart of Fig. 6 for the flame shape  $F(r, t) \equiv Rf(\eta, \tau)$  [Eq. (49)], showing that the flame front is distorted stronger in an incompressible flow, while gas compression reduces the flame surface area and as such moderates the flame acceleration.

According to Eq. (8), the scaled instantaneous total flame velocity with respect to the fuel mixture is  $\Omega_w(\tau) \equiv U_w/S_L = f(1, \tau)$ . In Fig. 8 we show  $\Omega_w$  versus time for  $Re=20, 30$  and compare the present prediction to previous numerical simulations of the initial stage of flame acceleration [6]. Comparing the theoretical plots for  $M_0=0$  (dashed) with that for  $M_0=10^{-3}$  (solid) also demonstrates that moderation in the flame acceleration becomes stronger with time. In both Figs. 8(a) and 8(b), the predictions with  $M_0=10^{-3}$  agree well with the numerical data, shown by symbols. We emphasize that such an agreement is quite encouraging, recognizing the restrictions of the present theory. In fact, the numerical results of Fig. 8 justify the model of the plane-parallel flow.

The moderating flame acceleration can be further demonstrated in the form of a differential equation for the average flame position. In the zeroth-order approximation of  $M_0$ , the

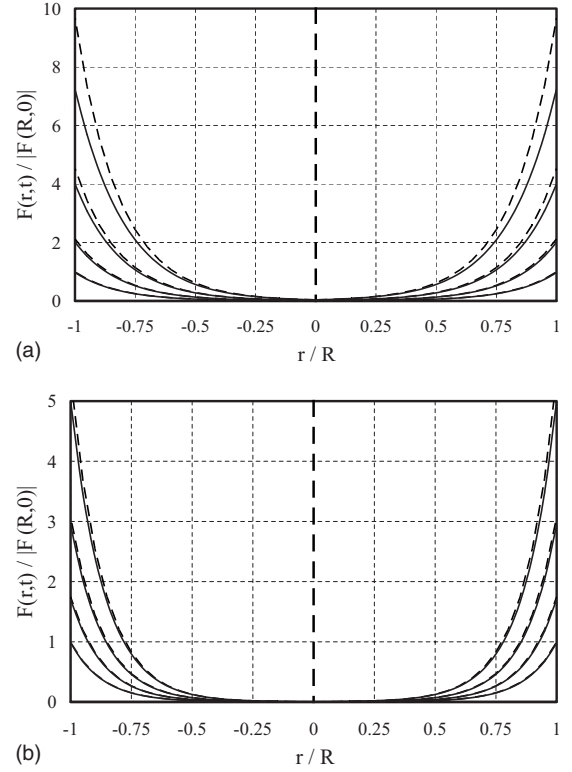


FIG. 7. Scaled flame shape [Eq. (49)] (a) for  $Re=10$  at the instants  $tS_L/R=0, 0.25, 0.5, 0.75$  and (b) for  $Re=100$  at the instants  $tS_L/R=0, 1, 2, 3$ , with the initial expansion factor  $\Theta=8$  and the adiabatic exponent  $\gamma=1.4$ .

accelerating flame dynamics is determined by the differential equation

$$\dot{\Sigma} = \sigma \dot{\Sigma}. \quad (59)$$

In the first-order approximation, Eq. (59) is modified as

$$\dot{\Sigma} = \sigma \dot{\Sigma} (1 - M_0 B \dot{\Sigma}), \quad (60)$$

with the coefficient  $B$  calculated from Eqs. (38) and (40) as

$$B = - \frac{\langle \alpha_2 \rangle (1 + S_2)}{\langle \alpha_1 \rangle^2 (1 + S_1)^2} = \left( \frac{\Theta - 1}{\Theta} \right)^2 A (1 + S_2). \quad (61)$$

Obviously,  $B \propto A > 0$ , so that Eq. (60) describes moderating flame acceleration. Integrating Eq. (60) with the initial condition  $\dot{\Sigma}(0) = \Theta / (1 + M_0 B \Theta) \approx \Theta$ , we find the ‘‘averaged’’ flame-front velocity in the laboratory frame and its position as

$$\dot{\Sigma} = \frac{U_L}{S_L} = \frac{\Theta \exp(\sigma \tau)}{1 + M_0 B \Theta \exp(\sigma \tau)}, \quad (62)$$

$$\Sigma = \frac{\langle Z_f \rangle}{R} = \frac{1}{\sigma M_0 B} \ln[1 + M_0 B \Theta \exp(\sigma \tau)]. \quad (63)$$

The solid plots in Figs. 9 and 10 present, respectively, Eqs. (62) and (63) for  $M_0=10^{-3}$  and various values of  $Re=10, 30, 100$ , while the dashed plots are the respective results in the incompressible limit,  $M_0=0$ . It is seen that the solid

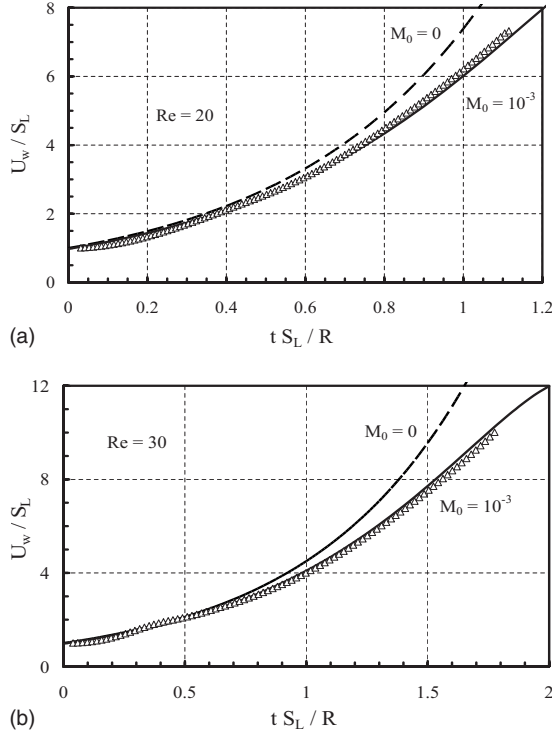


FIG. 8. Time evolution of the scaled total burning rate  $U_w/S_L$  for  $\Theta=8$ ,  $\gamma=1.4$  and (a)  $Re=20$  and (b)  $Re=30$ . In both figures, the theoretical predictions for  $M_0=0$  (dashed) and  $M_0=10^{-3}$  (solid) are compared to the numerical simulations [6] shown by symbols.

and dashed plots overlap with each other only during the initial stage of burning,  $M_0 \exp(\sigma\tau) \ll 1$ , when gas compression is unimportant. In contrast, in the opposite limit of  $M_0 \exp(\sigma\tau) \gg 1$ , Eqs. (62) and (63) yield steady flame propagation with  $\dot{\Sigma}=1/(M_0B)$ .

Consequently, Eqs. (62) and (63) reproduce qualitatively the main stages and tendencies obtained in experiments and numerical simulations, as shown in Figs. 1 and 2. Indeed, we observe in Fig. 9 the initial exponential regime of flame acceleration, which is followed by moderated flame acceleration and eventually by steady flame propagation.

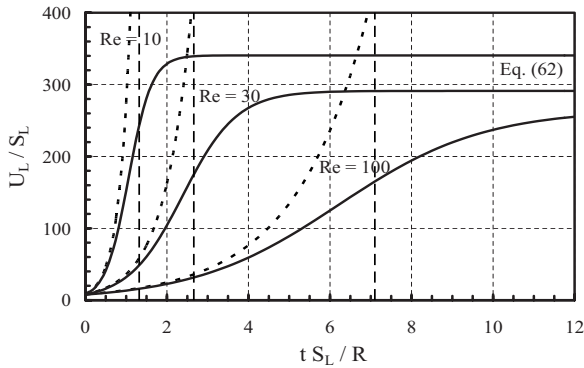


FIG. 9. Evolution of the averaged flame velocity in the laboratory frame for  $\Theta=8$ ,  $\gamma=1.4$ , and  $Re=10, 30, 100$ . Equation (62) with  $M_0=0$  and  $M_0=10^{-3}$  describes the dashed and solid plots, respectively. The vertical lines are related to the validity limits  $\sigma\tau \approx 4$ .

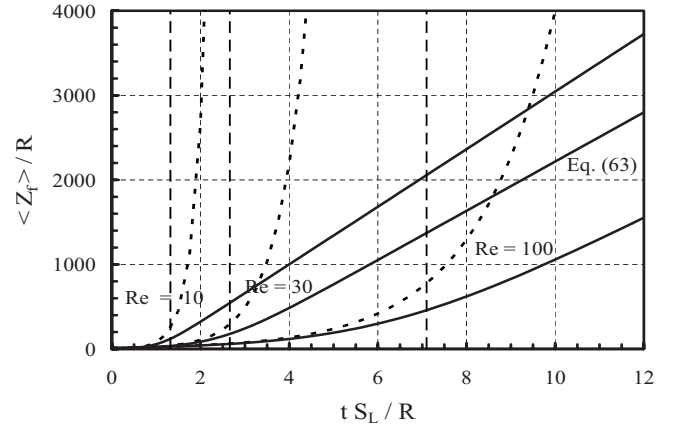


FIG. 10. Evolution of the averaged flame position for  $\Theta=8$ ,  $\gamma=1.4$ , and  $Re=10, 30, 100$ . Equation (63) with  $M_0=0$  and  $M_0=10^{-3}$  describes the dashed and solid plots, respectively. The vertical lines are related to the validity limits  $\sigma\tau \approx 4$ .

We next note that even the regime of moderated almost constant flame acceleration is beyond the approach of weak compressibility, the present theory can still be used for order-of-magnitude evaluations. As estimation, we calculate the maximum possible value of the flame acceleration from the condition  $\ddot{\Sigma}=0$ . According to Eq. (62), this condition is satisfied at the instant

$$\tau = -\sigma^{-1} \ln(M_0 B \Theta), \quad (64)$$

which is related to the bending points of solid plots in Fig. 9, and the maximum acceleration is given by

$$\ddot{\Sigma}_{\max} = (\dot{U}_L R / S_L^2)_{\max} = \sigma / (4M_0 B). \quad (65)$$

In Fig. 11 we compare Eq. (65) (solid) to the numerical data [18] represented by symbols. It is seen that although the theoretical prediction shows qualitatively the same moderating tendency as the numerical results, Eq. (65) yields values that are smaller than those of the numerical simulation by almost a factor of 2. Consequently, the present theory provides only qualitative order-of-magnitude estimate for the acceleration value in the regime of almost constant flame

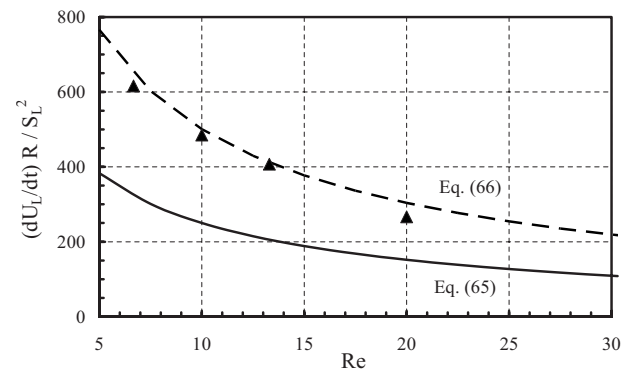


FIG. 11. The maximal value of the flame acceleration versus the Reynolds number: the theoretical prediction of Eq. (65) (solid), the empirical Eq. (66) (dashed), and the simulation results [18] (symbols).

acceleration. We note nevertheless that the theory would quantitatively agree with the numerical results if we multiplied Eq. (65) by an empirical factor of 2 in that

$$\ddot{\Sigma}_{\max}^{\text{emp}} = (\dot{U}_L R / S_L^2)_{\max}^{\text{emp}} = \sigma / (2M_0 B), \quad (66)$$

as shown by the dashed plot in Fig. 11. The close agreement between Eq. (66) and the simulations [18] may be useful for future studies.

As for the last stage of flame propagation, on the basis of the classical theory [16,17], we expect the steady flame speed to be about the Chapman-Jouguet (CJ) deflagration speed in the laboratory reference frame, i.e.,  $U_{\text{CJ}} \approx (2-3)c_0$  (see also Fig. 2). On the other hand, Eq. (62) yields  $U_{L,\text{steady}} = S_L / M_0 B = c_0 / B$ . For the parameters of Fig. 9, i.e.,  $\text{Re} = 10, 30, 100$ ,  $M_0 = 10^{-3}$ ,  $\Theta = 8$ , and  $\gamma = 1.4$ , this value is about  $U_{L,\text{steady}} \approx (250-350)S_L = (0.25-0.35)c_0$ , which is one order of magnitude smaller than the respective velocity of CJ deflagration.

Consequently, the present theory agrees quantitatively with the numerical results during the first stage of flame acceleration when compressibility is relatively small. The theory provides also order-of-magnitude evaluations for the regime of almost constant flame acceleration when compressibility is considerable. Finally, in the limiting regime of fast quasisteady flame, the present theory yields only qualitative understanding of the process. Meanwhile, for all stages of flame acceleration we obtained the same tendency that gas compression moderates and finally suppresses the acceleration process.

## VI. CONCLUDING REMARKS

Recognizing that flame-generated compression waves play an important role in the reduction of flame acceleration [8,18], in the present work we have extended the theory of flame acceleration in an incompressible flow [6] to account for weak compressibility through expansion in small initial Mach number up to the first-order terms. We have derived and solved a set of equations [Eqs. (1), (7), (8), and (24)], which govern the evolution of the flame and the flow. As a result, we show that compressibility moderates the flame acceleration, modifying the entire process from the initial exponential regime to almost linear acceleration and then to steady deflagration. We have derived analytical formulas for the main characteristics of the flame dynamics such as the flame shape and speed, as well as the velocity profile in the flame-driven flow [Eqs. (48)–(57)]. The acceleration becomes stronger with the expansion factor and is reduced with increasing tube width.

The present theory is applicable to flame propagation with small  $\text{Re}$  and in good quantitative agreement with reported numerical results at the initial stage of flame acceleration during which gas compression is relatively small. It provides order-of-magnitude evaluations in the regime of almost constant flame acceleration when gas compressibility is considerable and yields qualitative understanding of the process in the limiting regime of fast quasisteady flame propagation.

## ACKNOWLEDGMENTS

We thank R. A. Yetter for the data of Fig. 1. This work was supported by the (U.S.) Air Force Office of Scientific Research, the Swedish Research Council (VR), and the Swedish Kempe Foundation.

- 
- [1] K. I. Shelkin, Zh. Eksp. Teor. Fiz. **10**, 823 (1940).
  - [2] A. K. Oppenheim, Philos. Trans. R. Soc. London, Ser. A **315**, 471 (1985).
  - [3] Ya. B. Zeldovich, G. I. Barenblatt, V. B. Librovich, and G. M. Makhviladze, *Mathematical Theory of Combustion and Explosion* (Consultants Bureau, New York, 1985).
  - [4] E. S. Oran and V. N. Gamezo, Combust. Flame **148**, 4 (2007).
  - [5] G. Ciccarelli and S. Dorofeev, Prog. Energy Combust. Sci. **34**, 499 (2008).
  - [6] V. Bychkov, A. Petchenko, V. Akkerman, and L. E. Eriksson, Phys. Rev. E **72**, 046307 (2005).
  - [7] V. Akkerman, V. Bychkov, A. Petchenko, and L. E. Eriksson, Combust. Flame **145**, 206 (2006).
  - [8] M. Wu, M. Burke, S. Son, and R. Yetter, Proc. Combust. Inst. **31**, 2429 (2007).
  - [9] L. Kagan and G. Sivashinsky, Combust. Flame **134**, 389 (2003).
  - [10] D. Valiev, V. Bychkov, V. Akkerman, and L. E. Eriksson, Phys. Lett. A **372**, 4850 (2008).
  - [11] M. Kuznetsov, V. Alekseev, Yu. Yankin, and S. Dorofeev, Combust. Sci. Technol. **174**, 157 (2002).
  - [12] M. Kuznetsov, V. Alekseev, I. Matsukov, and S. Dorofeev, Shock Waves **14**, 205 (2005).
  - [13] C. Johansen and G. Ciccarelli, Combust. Flame **156**, 405 (2009).
  - [14] V. Bychkov, D. Valiev, and L. E. Eriksson, Phys. Rev. Lett. **101**, 164501 (2008).
  - [15] V. Gamezo, T. Ogawa, and E. Oran, Combust. Flame **155**, 302 (2008).
  - [16] L. D. Landau and E. M. Lifshitz, *Fluid Mechanics* (Pergamon Press, Oxford, 1989).
  - [17] R. Chue, J. Clarke, and J. H. Lee, Proc. R. Soc. London, Ser. A **441**, 607 (1993).
  - [18] D. M. Valiev, V. Bychkov, V. Akkerman, and L. E. Eriksson, Phys. Rev. E **80**, 036317 (2009).
  - [19] C. K. Law, *Combustion Physics* (Cambridge University Press, New York, 2006).